Electrotunable Lubrication with Ionic Liquids: the Effects of Cation Chain Length and Substrate Polarity

Silvia Di Lecce,*,† Alexei A. Kornyshev,† Michael Urbakh,‡ and Fernando Bresme*,†

†*Department of Chemistry, Molecular Sciences Research Hub, Imperial College, W12 0BZ London, U.K.*

‡*School of Chemistry and The Sackler Center for Computational Molecular and Materials Science, Tel Aviv University, Tel Aviv*

E-mail: silvia.di-lecce@imperial.ac.uk; f.bresme@imperial.ac.uk

Abstract

Electrotunable lubrication with Ionic Liquids (ILs) provides dynamic control of friction, with the prospect to achieve superlubrication. We investigate the dependence of the frictional and structural forces with 1-n,2-methyl-imidazolium tetrafluoroborate $[C_nMIM]^+[BF_4]^-$ (n=2,4,6) ILs as a lubricant, on the molecular structure of the liquid, normal load and polarity of the electrodes. Using non-equilibrium molecular dynamics simulations and coarse grained force–fields we show that the friction force depends significantly on the chain length of the cation. ILs containing cations with shorter aliphatic chains show lower friction forces, $\sim$ 40% for n=2 as compared to the n=6 case, and more resistance to squeeze-out by external loads. The normal load defines the dynamic regime of friction as well as it determines maxima in the friction force at specific surface

charges. At low normal loads, $\sim$ 10 MPa, the velocity profile in the confined region resembles a Couette type flow, while at high loads $>$ 200 MPa the motion of the ions is highly correlated and the velocity profile resembles is "plug" like. Different dynamic regimes result in distinctive slippage planes, located either at the IL-electrode interface or in the interior of the film, which ultimately lead at high loads to the observation of maxima in the friction as function of surface charge densities. Instead, at low loads the maxima are not observed, and the friction is found to monotonously increase with surface charge. Friction with $[C_nMIM]^+[BF_4]^-$ as a lubricant is reduced when the liquid is confined between positively charged electrodes. This is due to better lubricating properties and enhanced resistance to squeeze-out when the anion $[BF_4]^-$ is in direct contact with the electrode.

Keywords

Ionic liquid - Friction - Nanotribology - Lubricants - Non-equilibrium simulations

Introduction

Nanotribology, the science of friction at the nanoscale, attracts significant interest due to its importance in micro and nanoelectromechanical systems (MEMS/NEMS),[1,2] as well as in lubrication phenomena taking place at macroscopic scales, *e.g.* in engines and earthquakes.[3–5] Understanding the properties of lubricants under nano-confinement conditions is the key to predict the friction response.

Good liquid lubricants should comply with several requirements:[6,7] (i) the motion of the confined film in response to an external perturbation should be *reproducible*; (ii) when a pressure load is applied, the liquid lubricant should *resist squeeze-out*; (iii) the performance should be *robust* and independent from changes in environmental properties, such as temperature, pressure, shear stresses, contamination, etc. More recently, the attention has been

focused on the dynamic control of friction, *e.g.* by applying electromagnetic fields. This notion is at the heart of a new research area in friction, called tribotronics.[8]

Ionic Liquids (ILs) are receiving significant attention in tribology, either as lubricants[9] or lubricant additives.[7] ILs feature very low volatility,[6,9,10] a desirable property of lubricant, and they are resistant to squeeze-out upon applying external loads.[11–13] ILs are charged fluids, consisting of a mixture of cations and anions, hence they can interact with charged surfaces forming electrical double layers. This is a key feature in energy storage (supercapacitors), electrocatalysis, and tribotronic applications.[14] An example of the latter is electrotunable lubricity, whereby the properties of the IL are modified using external electric fields that lead to different friction states. The application of electrostatic fields to nanoscale films can induce states of super-low friction and wear (superlubricity states),[15,16] a highly sought property in nanotribology. The control of lubrication using electrostatic fields has been explored in aqueous solutions of sodium dodecyl sulphate surfactants.[17] However, the electrotunable lubricity with aqueous electrolytes is problematic, not only because of their volatility, but also due to the small electrochemical window of water. For ILs this window is, at least, twice as large, therefore providing a better scope for the development of devices based on electrotunable friction control.

Both experiments[11,18] and simulations[12,19] showed that nano-confinement between charged surfaces induces the ordering of ILs into layers of alternating charge. Generally, near charged surfaces, the response of ILs, ultra-concentrated solvent-free electrolytes, at small and moderate charges is characteristic of overscreening.[20] The different screening regimes result in a non-monotonic dependence of the friction force on the surface charge density.[12] Further, experimental studies with Surface Balance Apparatus (SBA) showed that under confinement ILs exhibit a quantized friction response,[16] and the friction coefficient varies with the number of confined layers.[11] The SBA experiments have also shown that the structure of IL confined between mica surfaces depends strongly on the ions composition. Pyrrolidium cations with short aliphatic chains form alternating cation-anion monolayers, while cations

with long aliphatic chains, typically above 8 carbon atoms, form interdigitated bilayers.[21] The boundary ionic layer next to the wall has predominantly a charge opposite to that on the surface, showing that the interfacial structure of the ions is determined to a large extent by electrostatic interactions, even for cations involving long aliphatic chains. The impact of different types of surfaces, silica and metallic, on the friction mediated by ILs has been studied using Atomic Force Microscopy (AFM),[2,16] demonstrating the impact of surface polarity on the friction force. The force increases or decreases depending on the sign of the surface potential.[15] Very recently, the mechanism of shear of ILs under nanoconfinement was investigated using atomic force microscopy.[22] These experiments revealed the formation of crystal structures, and provided support for the shift of the slippage plane from the solid-liqid interface to the interior of the film, a physical effect that has been predicted using non-equilibrium molecular dynamics simulations.[12]

Our group has performed a number of numerical simulations to unravel the microscopic mechanisms determining the friction response in terms of ionic liquid composition, surface charge and substrate roughness.[12,13,23] These simulations showed that the friction force features a maximum at a specific surface charge density, whose value depends on the load and substrate-IL interactions. We established that at high enough surface charges the shear plane shifts from the wall-IL interface to the inner region of the confined film, leading to a reduction of the friction at high surface charges. The SFB and AFM experiments mentioned above highlighted the important role of cation size on the layering of confined films, as well as the role of polarity of the confined surfaces on the friction force. The questions we address in this work are: (i) how does the friction force depend on the composition of the IL, in particular the size of the cation? (ii) How does the different structures of the confined liquids, and therefore the friction forces, can be electrotuned by changing both the surface charge and polarity of the confining electrodes? Answering these questions is important for building theoretical insights into the properties of confined ILs and for developing new electrotunable devices.

We focus our investigation on imidazolium ILs, changing systematically the length of the aliphatic chain of the cation $[C_nMIM]^+[BF_4]^-$, (n = 2, 4, 6), using a Coarse Grained (CG) model that we have recently tested.[24] The alkylimidazolium family of ILs have attracted significant interest in nanotribological studies,[2,6,7,25] and in electrochemical applications,[26] due to their low viscosity and high electric conductivity.

Methodology

Non-Equilibrium Molecular Dynamics (NEMD) simulations were performed using a simulation set–up that mimics experiments using the SFB and AFM.[12,13] The IL was confined between two solid slabs under a normal load, f_L, resulting in a total load $F_L = 2f_L$ on the liquid film, as shown in Figure 1. The normal load was applied by imposing an acceleration on each atom in the slabs, along the z-direction. The slabs were immersed in bulk IL, hence allowing exchange of molecules between bulk and confined regions, as a response to the normal pressure, temperature, or surface charge. Shear on the confined film was induced by pulling one of the slabs at a constant velocity through a spring with a force constant of $\sim$16 N m^{-1}, which is attached to a stage moving with a constant velocity of $v_{dir} = 5$ m s^{-1}. The other slab was kept fixed at its original position by using harmonic restraints, which were applied on every atom. Both slabs are periodic in the direction of pulling, y (see Figure 1). We investigated previously the dependence of the friction force on the sliding velocity (see Ref.[23]), showing that the friction force variation can be accurately described using the Eyring's activation model. All in all, the this system we investigate here is not expected to be in the linear regime.

The slabs were kept at 350 K by rescaling the velocities of the walls atoms only using the v-rescale thermostat.[27]No thermostat was applied to the Ionic Liquid. A normal load was first applied for 4 ns, and then, the confined region was subjected to shear by pulling at constant velocity as indicated above. The force acting on the pulled slab was measured at

every time step and the time average was computed (neglecting the first 100 ps) to obtain the friction force. Following the equilibration period, we performed a systematic analysis of the friction force as a function of the normal load. The structure of the film changes with the applied load, undergoing transitions to smaller thicknesses when the load is increased (see Figure 2 and Figure 3 (a)). To compute the average film thickness and friction force we ensured that the slab–slab distance was fluctuating around a well defined average.

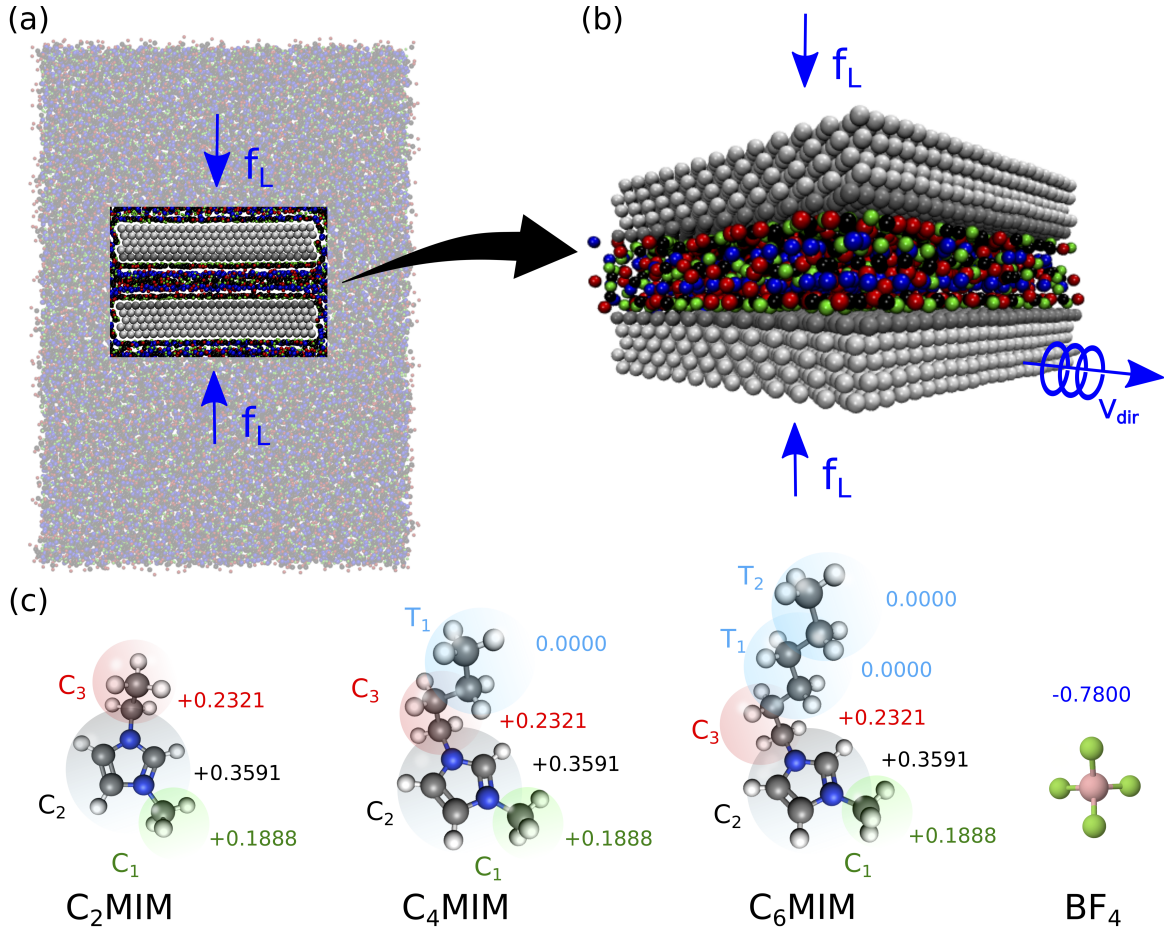

Figure 1: (a) Simulation set-up employed in this work, showing the confining slabs immersed in a fully periodic simulation cell, containing bulk IL. (b) Snapshot of the confined IL under a normal load f_L, acting on both slabs. One of the slabs moves along the y direction at constant velocity v_{dir}. The IL in the figure is $[C_2MIM]^+[BF_4]^-$, and it is confined between the solid plates with surface charge densities, –32 μC cm^{-2}. The atoms in the slabs are coloured in light gray (neutral atoms) and dark gray (charged atoms in contact with the IL). (c) The ionic liquids consist of C_nMIM, (n=2,4,6) cations and BF_4 anions modelled using a coarse grained force–field[24].

ILs were modelled using a Coarse Grained Force–Field (CGFF)[24] that describes the

family of 1-n-3-methyl-imidazolium tetrafluoroborate $[C_nMIM]^+[BF_4]^-$ IL (C_n = 2,4,6). We show in Figure 1 the mapping of the atomic structure of the IL into the CG one using beads. The beads interact through Lennard–Jones and Coulombic interactions as defined in Ref.[28] (see Table S1). For full details of the force–field and tests of its performance see Ref.[24]

A typical simulation involved the following procedure: the slabs were placed in the center of the simulation cell and solvated by adding the ions randomly. The number of cations/anions in the simulations was adjusted to reproduce the bulk density of the IL at the chosen thermodynamic conditions, in our case 350 K and 1 bar. We ensured that the density of the IL far from the solid–liquid interface corresponded to the chosen thermodynamic state. For bulk solutions at 1 bar, 350 K and the CGFF used in this work the liquid densities are: 1226.23 ± 0.033 kg m^{-3} for $[C_2MIM]^+[BF_4]^-$, 1170.64 ± 0.041 kg m^{-3} for $[C_4MIM]^+[BF_4]^-$ and 1108.26 ± 0.2 kg m^{-3} for $[C_6MIM]^+[BF_4]^-$,[24] in good agreement with the experiments. For charged slabs we adjusted the number of cations or anions to obtain electroneutral systems. The system was then equilibrated in the canonical ensemble (NVT).

The slabs were constructed by replicating a face–centered cubic {111} unit cell, with lattice parameter 0.36 nm. The atoms within the slab interact with each others through a Lennard–Jones potential, with effective diameter 0.32179 nm and interaction strength 50 kJ mol^{-1} . The strength of interaction between atoms in different slabs is set to 1 kJ mol^{-1}.[13] The Lennerd–Jones interactions are truncated at a cut-off radius of 1.2 nm. The atoms in the layer facing the confined region (see Figure 1) were used to define the desired surface charge of the slab, by assigning partial charges. One slab contains typically 2838 total atoms and 572 charged atoms. The atoms in the slab that is not moving (top slab in Figure 1 (b)) were restrained in the x and y directions using a harmonic potential with force constant of 10000 kJ mol^{-1} nm^{-2}. The same force constant was applied to the atom of the sliding slab (bottom wall in Figure 1 (b)) in the x direction, while the atoms were free to move in the shear direction, y. The atoms in both sliding and static slabs were free to move in the z direction, to allow the application of the normal load.

The velocity profiles of the confined IL were obtained from the analysis of the displacement of the IL molecules in the confined region. We computed the friction force for different surface charge densities, from –8 μC cm^{-2} to –50 μC cm^{-2}, and charge set-ups, negatively (–,–), positively (+,+) and oppositely charged electrodes (+,–), to assess the role of the electrode polarity on the friction force. As a reference, the surface charge density of mica in aqueous electrolyte solutions is estimated as –32μC cm^{-2}.[29,30]

Long range electrostatic interactions were computed using the particle-mesh Ewald summation method (PME)[31], with "tinfoil" boundary conditions, *i.e.* the system is embedded in a perfect conductor medium. The ionic liquid itself is only ionically conductive, but not electronically conductive. The dielectric constant for the electrostatic interactions was set to $\varepsilon_r = 1$. We could do this, because the partial charges of ions in our model of IL were rescaled to take into account the electronic polarizability of the ions, therefore we do not need to introduce an effective dielectric constant to take into account the electronic degrees of freedom of the liquid. The cross interactions between sites of two different types, i and j, were calculated using the Lorentz–Berthelot combining rules, namely $\sigma_{ij} = (\sigma_i + \sigma_j)/2$ and $\varepsilon_{ij} = \sqrt{\varepsilon_i \varepsilon_j}$. Following our previous works, the Lennard–Jones interactions for the atoms in the solid blocks was set to $\varepsilon_s = 22.5$ kJ mol^{-1}. These interactions were used to derive the pair interactions between the atoms in the slabs and the atoms in the ILs using the combining rules. These interactions were fitted in our previous work to reproduce the wettability behavior of ILs on the mica surface.[13] While the compressibility of the ILs depends on the magnitude of the dispersion interactions, the key microscopic mechanism of friction, namely the observation of maxima in the friction force, is independent on the strength of the disperion interaction. We have investigated this question in Ref.[23] The molecular dynamics package, GROMACS v.5.1.4,[32,33] was employed in all our simulations.

The friction force was computed using films of varying thicknesses, corresponding to different load conditions. The slab–slab separation decreases during the first nanoseconds of the simulation, squeezing out layers of the ionic liquid and restructuring of the ionic liquid

film. In the Supporting Information (see Figure S1) we show an example of the dependence of the slab-slab distance with normal load, for a representative IL ($[C_4MIM]^+[BF_4]^-$ at 350 K, normal load 200 MPa and surface charge density of –32 μC cm^{-2}). The averages of the properties reported below were obtained by analyzing "stable" films, whose thickness (number of IL layers) does not change for at least 8 ns.

Note that the squeeze out process in our simulations, namely the ejection of 2 layers, takes place when the pressure reaches the maximum pressure defining the limit of mechanical stability of the film. Very close to the maximum in pressure a fluctuation to can bring the film to a thinner state. The thinning process is diffusion limited and the simulations should be performed over long-time scales to ensure the thinning is complete. To obtain reproducible structural forces we performed simulations using as starting point a thick film, which was compressed systematically by increasing the load. As noted in our work we found that simulations with timescales over 10s of ns are necessary to achieve stable film thicknesses (see Figure S1).

Results and Discussion

Dependence of structural and friction forces on the alkyl chain length of the cation

ILs confined between charged surfaces of the same polarity structure themselves into an odd number of layers. The density profiles shown in Figure 2 illustrate this idea for negatively charged surfaces, –32 μC cm^{-2}. The layering results in distinctive structural forces, whose origin can be investigated by computing the pressure–distance isotherms (see Figure 3 (a)). The isotherms feature discontinuous jumps and are similar to those obtained in experiments with the SFB.[11] The discontinuous jumps are connected to the packing of the ions inside the confined space. IL layers are squeezed–out in pairs (see Figure S1), an observation that is consistent with electroneutrality arguments, and in agreement with the behavior inferred

from SFB experiments[11] and from previous simulations[13] using other ILs. This behavior is observed for all the ILs investigated here, indicating that even for the cations with longer chains, C_6MIM, the electrostatic interactions play a dominant role in defining the structure of the confined liquid.

However, structural forces show distinctive quantitative differences across different ILs. Larger cations render films that are more compressible. This effect can be observed in the structural forces obtained both at low and high loads. At low loads P<200 MPa and large slab–slab separations (d>3 nm), the compression of C_6MIM results in thinner films. This observation is connected to the loss of two ion layers (see Figure 2). The same effect is observed at higher loads (see *e.g.* P>200 MPa and d< 2 nm) with the films involving larger cations, $C_{4,6}$MIM, become thinner than those for C_2MIM for the same load. The resistance against squeeze–out decreases in the order C_2MIM > C_4MIM > C_6MIM.

The analysis of the structure of confined films helps to get insights into the microscopic origin behind the resistance to squeeze–out. The smaller cations are more compact and they favor strong ordering into layer of alternating charge, even for thick films (see Figure 2). For larger ions, the aliphatic chains impose constrains on the space available for the counter ions to relocate in the film. Indeed, even at relatively low normal loads (see C_6MIM at 100 MPa in Figure 2) the anions are adsorbed next to the charged head group of the cation (C_1, C_2 and C_3), and the interior of the film is filled mostly by the aliphatic chains, which prevent the adsorption of anions in that region. The surface charge at the surface of the slabs induces the formation of alternating polar/non–polar structures. This notion can be assessed by performing simulations of the IL confined between neutral walls. Our simulation for zero surface charge show that both polar and non–polar groups populate the surface, forming in-plane nanodomains (see Figure S2).

The segregation of charged and polar regions inside the film is reminiscent of the formation of nano-domains, discussed before in the context of full atom and CG simulations,[24,34] where charged and non-polar regions segregate from each other forming the domains. The affinity

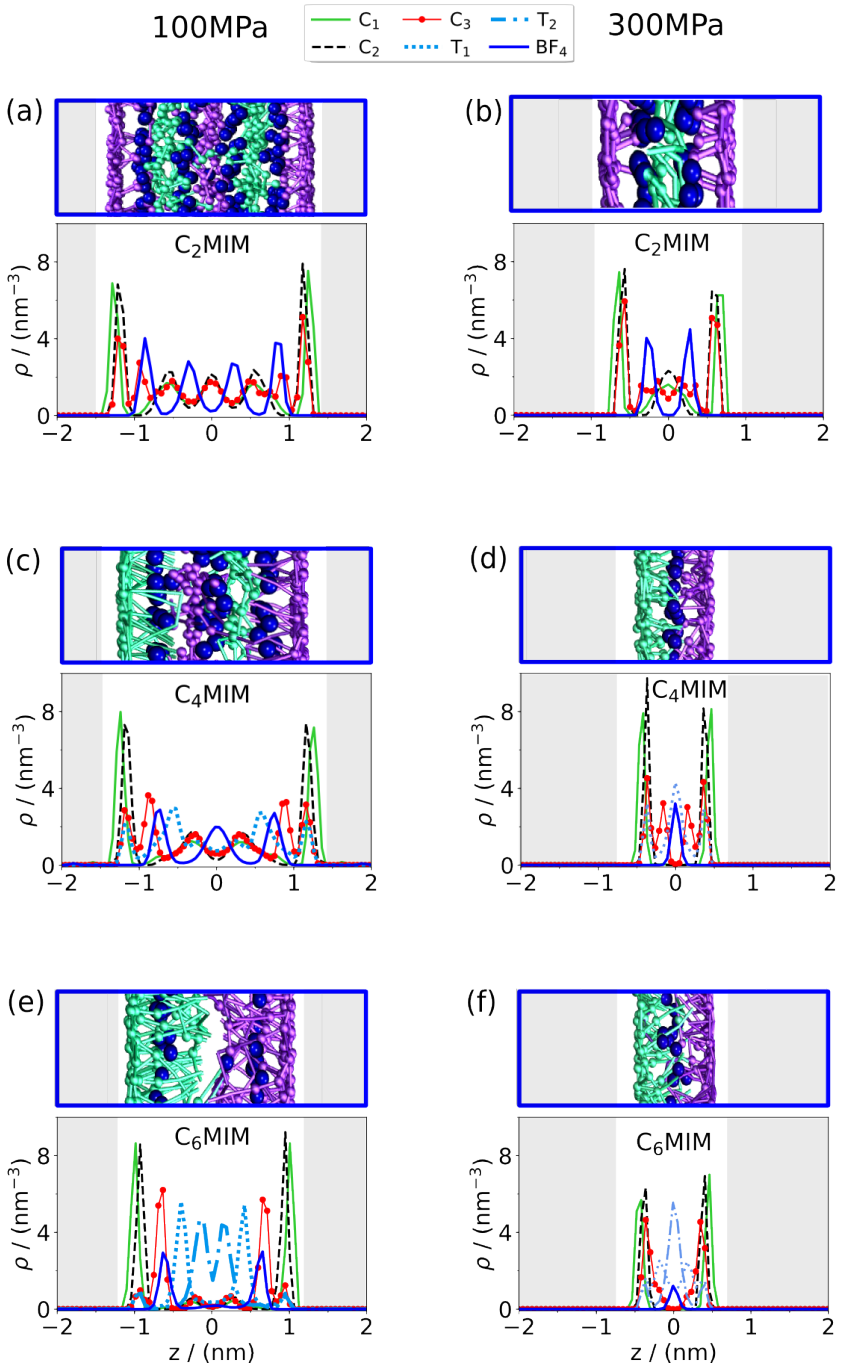

Figure 2: Number density profiles of the confined IL under external loads of 100 MPa and 300 MPa. (a-b) C_2MIM, (c-d) C_4MIM, (e-f) C_6MIM. The lines represents the number density of each group in the IL, as specified in the legend. All the results correspond to a surface charge density of –32μC cm^{-2} and 350 K. The snapshots show representative configurations of the ILs. Anions, BF_4, are represented as blue spheres. Cations located in different layers are coloured in purple and green.

to segregation observed for small and large cations explains the different compressibilities observed in our results, as well as the energy penalty for anions to populate the interior of the confined region (see results for the C_6MIM cation at 100 MPa and 300 MPa in Figure 2).

At very high pressures the interior of the $C_{4,6}$MIM films consists of two layers of cations only (see Figure 2(f)), which are directly adsorbed via their head groups to the negative surface. The pressure–distance isotherms show that this structure is very stable and can resists to significant loads, of at least 0.6 GPa (see Figure 3 (a)).

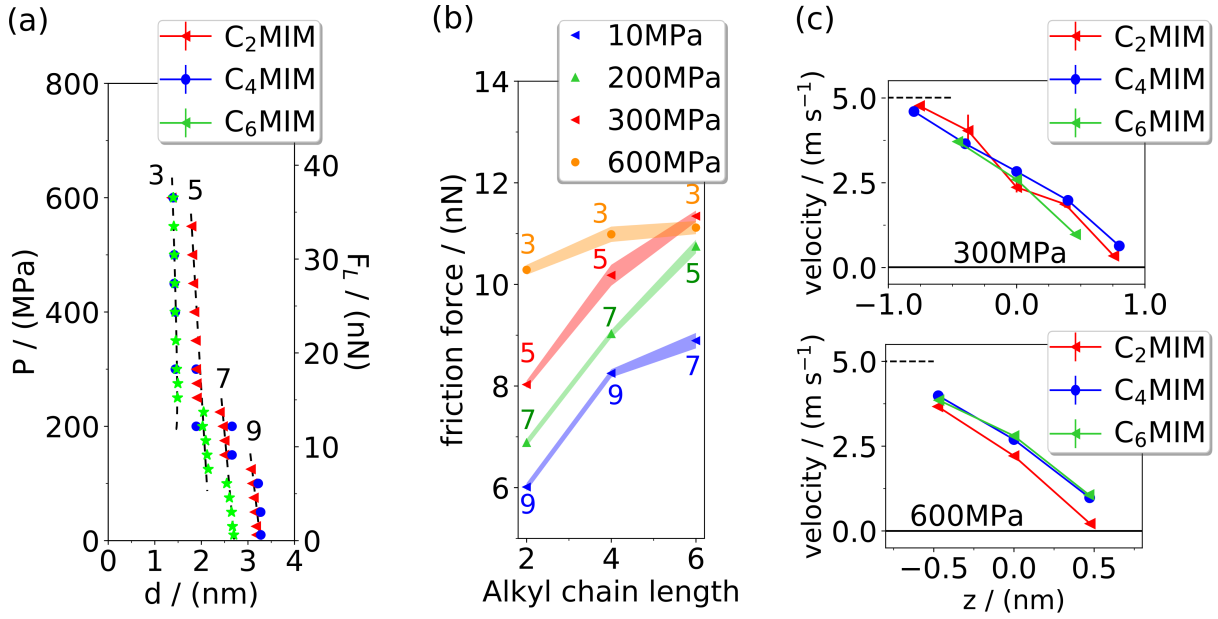

Figure 3: (a) Pressure-distance isotherm for the different ILs investigated in this work. (b) Friction force as a function of the alkyl chain length for different normal loads. (c) Velocity profiles of the confined ILs for different chain alkyl length and pressures as specified by the legend. The solid and dashed horizontal lines indicate the velocity of the slabs, 0 and 5 m s^{-1}. All the results were obtained using two negatively charged slabs, –32 μC cm^{-2} at 350 K. The numbers in panels (a) and (b) indicate the number of IL layers in the confined region.

The friction force increases with the size of the alkyl chain of the cation (see Figure 3(b)). The largest increase, about 40%, is obtained for the thicker films (lower loads) while at high loads (600 MPa) the friction is very similar for the three ILs. This is consistent with the film thickness obtained at this pressure, which is fairly independent on the alkyl chain length (see Figure S3). Otherwise, at normal loads of 10–300 MPa the C_6MIM ILs film is significantly thinner than the C_2MIM and C_4MIM films, and, consistently, a higher friction forces are

observed (see Figure 3(b)).

In contrast to smooth sliding, predicted by macroscopic hydrodynamic theory, the vast majority of friction experiments with nanoscale ionic liquid films, as well as our simulations, exhibit stick-slip motion. In this nonlinear dynamical regime, the frictional energy dissipation is completely determined by the sliding potential energy landscape experienced by the slider, and the contribution of viscous dissipation is minor.[35] We can compare the friction force calculated in simulations, F_{sim}, with the one, F_{calc}, obtained using the classical equation,

$$F_{calc} = \eta A \frac{v_{dir}}{d} \tag{1}$$

which assumes a linear velocity profile between two surfaces of area A separated by a distance d, with one surface moving at velocity v_{dir} , while the other surface is not moving, and the fluid has a viscosity η; this approximation corresponds to a Couette type flow. In Figure S4 we compare the force calculated via the equation above with the force obtained in the present simulations for $[C_nMIM]^+[BF_4]^-$ (n = 2,4,6) ILs, using the bulk viscosities reported in Ref.[24] While the dependence of the friction force on the alkyl chain length appears similar, this is so only for low pressures, which correspond to thicker films. At high pressure the calculated and simulated results do show different behaviors. The magnitude of friction forces obtained from the "calc" and "sim" approaches are also very different highlighting a breakdown of the classical hydrodynamic theory at the nano-sized gaps.

Recent experiments[18] suggest that the shear mechanism might be complex when cations with long alkyl chains (such as pyrrolidinoum, $C_{10}C_1$Pyrr) are considered, with possibly 3 shear planes playing a role, namely, (1) wall-IL, (2) between the cation/anion layers (ionic-plane), and (3) between alkyl chain/alkyl chain. The latter would arise from the interdigitation (bilayer formation) taken place in the interior of the ionic liquid. The alkyl chains investigated in the present work are much shorter than C_{10}, and at the surface charge density, –32 μC cm^{-2}, and the pressures considered here, the velocity profiles conform to a Couette

type regime (*i.e.* see Figure 3 (c) C_2MIM film at 300MPa). We will see below that this regime is very sensitive to the surface charge, and a more complex behavior is observed due to the synergistic effects between surface charge and normal load.

Overall, our results indicate that small ions are more lubricating than the larger ones. They feature a stronger layered structure that is more resilient to squeeze–out and favor thicker films for the same normal load. We find that this advantage is lost at very high pressures, above 600 MPa, for which the distances between the slabs including different ion types become very similar (see Figure S3). In that case the friction force only slightly depends on with the cation size.

Dependence of the friction force on the charge of the electrode

Previous experiments and simulations showed that the lubrication properties of ILs vary with the surface charge of the confining plates[13,15,16,19] opening a route to modify the friction force, dynamically. The surface charges change the preference of the ions to adsorb at the electrodes and modulate the layering structure in the confined film, shifting the position of the slippage plane and finally the magnitude of the friction force. Experimental studies of multilayer films used dielectric surfaces mostly, like mica, silica, or sapphire, for which an accurate control of the surface charge is impossible.[6] In those systems, the surface charge is defined by the detachment of ions from the surface into the confined region. Mica walls, for example, become negatively charged and the surface charge is believed to be close to –32 μC cm^{-2}.

To assess the impact of the normal load, IL composition and surface charge on the friction force, we focus our discussion on $[C_6MIM]^+[BF_4]^-$. The main result of this section is presented in Figure 4(a). We have included results for the friction force of $[C_2MIM]^+[BF_4]^-$ and $[C_4MIM]^+[BF_4]^-$ in Figure S5 that show the same behavior.

At high normal loads 100 MPa and 300 MPa, the friction force features a non–monotonic behavior with surface charge, showing a maximum at a specific charge density. This result

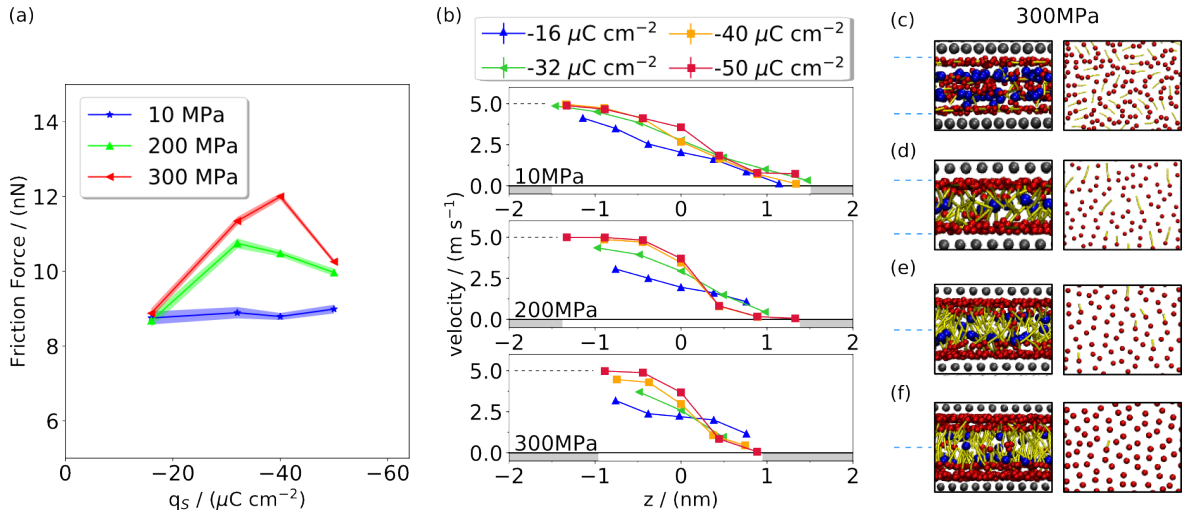

Figure 4: (a) Dependence of the friction force of $[C_6MIM]^+[BF_4]^-$ on the surface charge and normal load applied on the slabs. The shadowed areas around the lines joining the data represent the estimated uncertainty in the data. (b) Velocity profiles of the IL at different charge densities and loads, as indicated by the legend. The grey shadowed regions at the bottom of each panel, indicate the position of slabs. The error bars associated to the data are smaller than the symbol sizes. Front view (left panels) of the confined ILs at 300 MPa, and top view (right panel) of the first layer next to the moving wall for different charge densities: –16 (c), –32 (d), –40 (e) and –50 (f) μC cm^{-2}. The three atoms in the charged head group of the cation are represented as red spheres. The blue spheres represent the anion and the cation aliphatic tails are coloured in yellow. At higher surfaces charges (e) and (f) most tails are aligned in the direction perpendicular to the slab plane. The dashed line indicates the slippage plane according to the velocity profiles represented in panel (b).

confirms previous observations using primitive[12] and CG models of $[C_4MIM]^+[PF_6]^-$.[13] As observed in those works the maximum results from the interplay between the increase of the roughness of the energy landscape with surface charge, and the shift of the slippage plane from the solid–liquid interface to the interior of the film. We demonstrate in this work that the position of the slippage plane and the maximum in the friction force depend on the normal load (see Figure 4).

The friction force changes more significantly at higher loads (*c.f.* results for 10 MPa and 300 MPa in Figure 4). At lower normal loads, 10 MPa, the friction force does not feature a maximum, and it depends only slightly on the charge density. At this low pressure the confined film is thicker, and the velocity profile conforms to a Couette type. The velocity profiles change slightly with the charge density (see Figure 4 (b) top panel) and the first IL layer next to the solid moves close (at –16 μC cm^{-2}) or at the same velocity of the wall (for surface charges $>$ –16 μC cm^{-2}). When the IL is under a high load the flow profile changes significantly, resembling a plug like profile. At low surface charges, –16 μC cm^{-2}, and high loads, 300 MPa, the IL moves as a block inside the confined region (see Figure 4 (b) bottom panel). An intermediate state between Couette and plug can be observed for slightly lower pressures (see –16 μC cm^{-2} and 200 MPa in Figure 4), suggesting the transition between these two types of flows modes takes place continuously upon applying the load.

Clearly, the magnitude of the normal load plays a key role in the appearance of the maximum in the friction force. Thin films, and therefore high loads, are needed to induce the plug flow at low surface charges, which shifts to a Couette type flow at high surface charges. The transition between these two regimes is reached at lower surface charges the lower the pressure, leading to a shift of the maximum to lower surface charges for low loads, and eventually to the disappearance of the maximum for very low loads, when the film is thicker and the IL flow conforms to a Couette type for all surface charges.

We have represented in Figure 4 (c-f) representative snapshots of the structure of the confined film at high pressure, 300 MPa, and varying surface charge, where the maximum is

observed (see Figure 4(a)). The configuration shows clearly the strong impact of the surface charge on the orientation of cations, which tilt with increasing surface charge. This notion is very clearly illustrated by the snapshots showing the cation layer in contact with the slabs. The cations lie flat at the substrate at low surface charges, while they become essentially vertical at high surface charge. This creates a non–polar region inside the film, as discussed in the previous section, which prevents the adsorption of the anions in the middle of the film, and that defines the slippage plane, reducing the friction at high surface charges.

The snapshots (see right panels in Figure 4 (c-f)) also show that the C_6MIM cations in direct contact with the charged surface do not form a crystalline lattice (see Figure 4 (c-f)). This behavior is different from that reported using simpler models of ILs consisting of spherical ions,[12] which were found to form ionic crystals under confinement conditions. Hence, the molecular structure matters.

Dependence of the friction on the polarity of the electrodes

We have shown above a direct correlation between the friction force and the position of the slippage plane. The polarity of the electrode biases the adsorption behavior of the cations and anions in direct contact with the electrode, and therefore it is an important variable in electrotunable lubrication. It has been demonstrated using AFM experiments that the friction force can be tuned by changing the electrode polarity.[15]

We investigate the dependence of the friction force and the structure of the IL film on the polarity of the electrodes, by simulating positively, negatively and oppositely charged slabs. We have focused our discussion on the C_6MIM IL, surface charge density $|q_s| = 32$ μC cm^{-2} and 300 MPa. Additional results using shorter chains $C_{2,4}$MIM are presented in Figure S6. We show in Figure 5(a) the charge compensation for different ionic layers. The polarity modifies the electrostatic structure of the film. Similarly charged electrodes (negatively or positively) induce the structures with an odd number of layers, while we observe an even number of layers for oppositely charged electrodes (see Figure S7 for representative

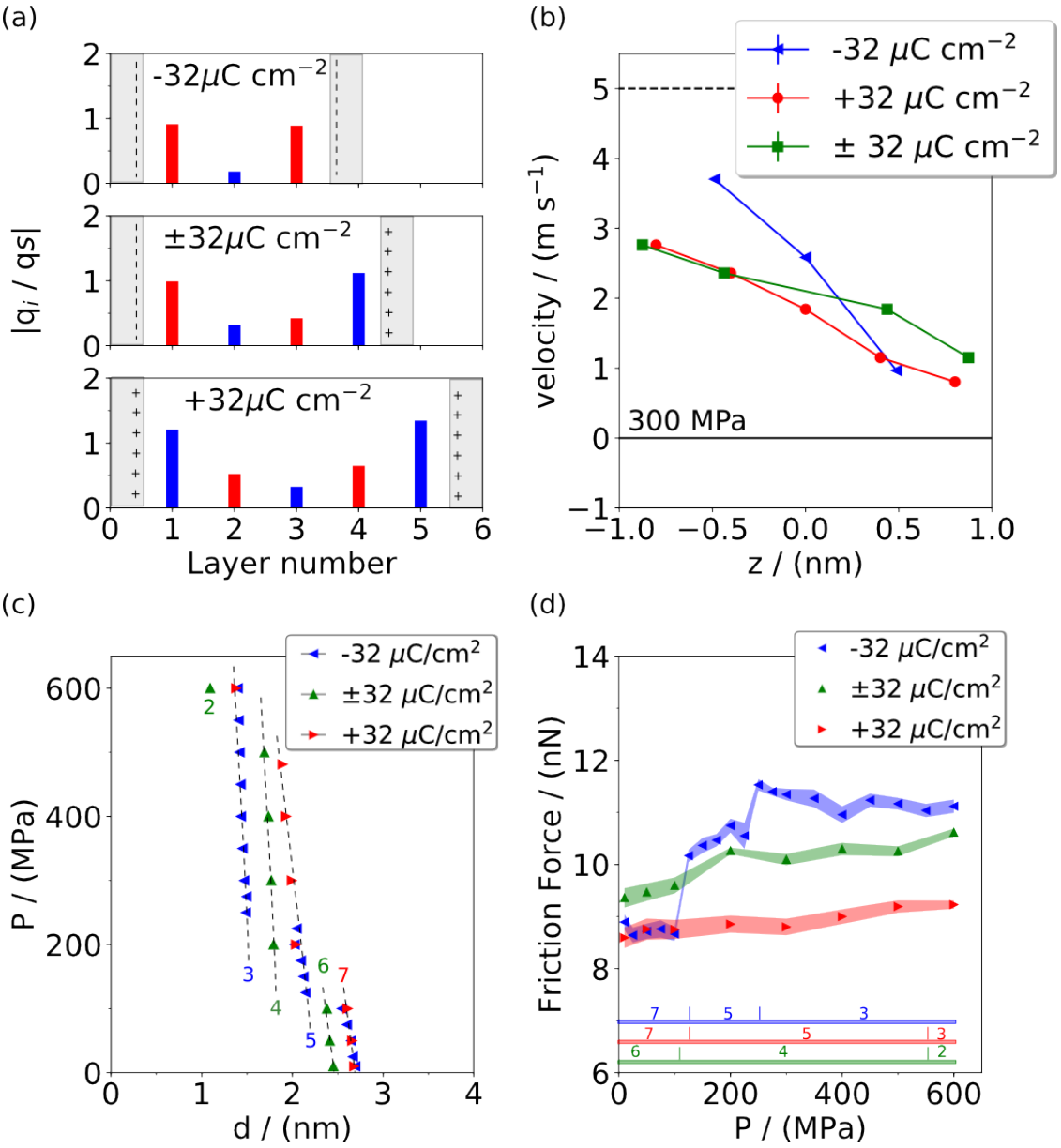

Figure 5: The tribological response of $[C_6MIM]^+$ $[BF_4]^-$ ionic liquid confined between electrodes with positive/positive (red right triangle), positive/negative (green up triangle), and negative/negative (blue left triangle) charges. (a) Charge densities of cation (red) and anion (blue) rich layers normalized by the surfaces charge density, q_s. All the data were obtain at 300 MPa. (b) Velocity profiles inside the IL film for the systems represented in panel (a). The error bars are smaller than the symbol size. In the positive/negative case, the slab with negative charge moves at constant velocity, while the slab with positive charge does not move. c) Pressure-film thickness isotherms for ILs confined between different electrodes. d) Friction force as a function of normal load. The numbers indicate the number of ILs layers for the different systems, as specified by the colors.

snapshots illustrating this idea). This result is consistent with the behavior expected from standard electrostatic (electroneutrality) arguments. At this high surface charge density we do not observe significant overscreening, namely, $|q_i/q_s| \sim 1$ for the layers in contact with the electrodes (see Figure 5(a)). Similar results are obtained for the $C_{2,4}$MIM cations (see Figure S6). This result is consistent with previous studies using primitive models consisting of spherical ions.[12] Significant overscreening was observed in that case at lower surface charges, only, as expected.[20]

We analyze in Figure 5(b) the friction mechanism, by computing the velocity profiles inside the confined region. All the systems feature a mixed type flow, between plug and Couette, hence showing some degree of boundary slip, and at these surface charges the dissipation still takes place at the wall-IL interface. Therefore, it is expected that the friction force will change with the composition of the monolayer (either cation or anion) in direct contact with the electrode. Our simulations indicate that in general ILs confined between positively charged electrodes lead to lower friction forces than those obtained with negatively charged electrodes. Hence, the anion layers in contact with the electrodes provide a better lubrication (see Figure 5 (d)). This result highlights a relative advantage of positive electrodes over negative ones in enhancing the lubrication properties of $[C_6MIM]^+$ $[BF_4]^-$. It should be noted that this conclusion depends on the nature of cations and anions and confining surfaces, which define a strength of ion-surface interactions and commensurability/incommensurability between the ionic sizes and surface periodicity.

The impact of the polarity on the structural forces is examined in Figure 5(c). These forces confirm our conclusion that positively charged electrodes favor thicker films, and, therefore, positive electrodes represent a better alternative to prevent squeeze–out. Indeed, squeezing the film from 5 to 3 layers requires pressures of the order of 200 MPa for the negatively symmetrically charged surfaces, while this pressure increases more than twice ($\sim$ 500 MPa) for positively charged surfaces. The system with oppositely charged surfaces features an intermediate behavior. The dependence of the film thickness on the electrode

polarity has a large impact on the friction force. At high normal loads, >100 MPa, the friction for positively or negatively charged surfaces is respectively lower or higher, with the system corresponding to oppositely charged slabs featuring again an intermediate behavior. This result can be understood considering the structural forces. For the same applied load, positively charged surfaces result in thicker films (containing larger number of layers), and consequently lower friction force. For lower normal loads (<100 MPa) the friction is less dependent on the polarity. This result is consistent with the structural forces presented in Figure 5(c), which shows that the films confined between positively or negatively charged surfaces have the same thickness (see Figure 5 (d)). The friction force recorded for the IL confined between oppositely charged slabs, is higher than in like charged surfaces case. This result is consistent with the formation of a thinner film between unlike charged surfaces (see Figure 5 (c)). We find that this behavior is fairly general and reproduced in ILs with smaller cations (see Figure S6).

Finally, comparison of the friction forces obtained with the three different cations shows that the smaller friction forces are obtained with $[C_2MIM]^+[BF_4]^-$, again highlighting the better lubricating properties of this IL and better resistance against squeeze–out when a normal load is applied on the IL film (see Figure S6).

Conclusions

We have performed coarse grained molecular dynamics simulation of the electrotunable friction with imidazolium ILs ($[C_nMIM]^+[BF_4]^-$, (n=2,4,6)) as lubricants, confined between electrodes at nanometer distances. The conclusions of this study are as follows:

• The structure of the cation influences the structural forces and the friction force. For the same load the friction force increases up to 40%, when the aliphatic chain length increases from C_2 to C_4. Cations with short aliphatic chains are therefore better lubricants. ILs consisting of smaller cations are also more resistant to the squeeze-out induced by external

loads.

• The friction force depends strongly on both the charge of the confining electrodes and the normal load. At low normal loads, ∼10 MPa, the friction force increases with the surface change. At high pressures, >200 MPa, we observe a maximum in the friction force at a specific surface charge. This is a general behavior, independent of the composition of the ILs studied here, and confirms previous studies using other CG ILs force–fields.

• The dependence of the maxima in the friction force on the normal load can be understood by analyzing the velocity profiles of the confined films. Under high loads, the motion of the ions in the confined region is highly correlated, and they move together at the same speed in a "plug" like profile fashion. At lower pressures the flow resembles a typical Couette profile. This result demonstrates that the friction response of the ILs is determined by a transition in the flow dynamics, from plug type for surface charges smaller than those corresponding to the maximum, to Couette like, for higher surface charges. For these transitions to take place high loads are essential, since only in this case the ions in the IL film form a highly correlated structure that moves as a single unit. These observations are reproduced across all the systems investigated in our work, showing that the flow mechanism described here might be a generic feature of IL lubricants.

• The lubrication properties of the ILs can be enhanced by modifying the polarity of the electrodes. The ILs consisting of cations, which are larger than anions, when confined between positively charged surfaces result in lower friction forces, about 30% lower, than the friction obtained with these ILs when they are confined between negatively charged surfaces. Positively charged electrodes induce electrosorption of BF_4 anions. These anions provides a better lubricating layer and reduced friction. The electrodes with opposite charges feature an intermediate behavior between that observed using like charged electrode.

These results rationalize the microscopic mechanisms of the electrotunable friction, and suggest avenues to tune friction using IL lubricants. For the $[C_nMIM]^+[BF_4]^-$, (n=2,4,6) the optimum response, defined as the lowest friction force, is achieved with small cations,

n=2, confined between positively charged electrodes. This result highlights the importance of the molecular structure of the ions in defining friction. Future extensions of this work will consider other compositions, targeting non-spherical anions and solvents, which are of interest in current experimental studies, as well as systematic analyses of the same questions using constant potential simulation schemes.

Acknowledgement

We acknowledge the award of a Research Grant by The Leverhulme Trust (RPG-2016-223). M.U. acknowledges the financial support of the Israel Science Foundation, Grant No. 1141/18, and of the Deutsche Forschungsgemeinschaft (DFG), grant no. BA 1008/21.

Supporting Information Available

The Supplementary Information contains data on the dependence of the friction force on the charge density and the polarity of the slabs for $[C_nMIM]^+[BF_4]^-$, (n=2,4).

References

1. Urbakh, M.; Klafter, J.; Gourdon, D.; Israelachvili, J. The Nonlinear Nature of Friction. *Nature* **2004**, *430*, 525–528.

2. Li, H.; Rutland, M. W.; Atkin, R. Ionic Liquid Lubrication: Influence of Ion Structure, Surface Potential and Sliding Velocity. *Phys. Chem. Chem. Phys.* **2013**, *15*, 14616–14623.

3. Scholz, C. H. Earthquakes and Friction Laws. *Nature* **1998**, *391*, 37–42.

4. Bayart, E.; Svetlizky, I.; Fineberg, J. Rupture Dynamics of Heterogeneous Frictional Interfaces. *J. Geophys. Res.: Solid Earth* **2018**, *123*, 3828–3848.

5. Rubinstein, S. M.; Barel, I.; Reches, Z.; Braun, O. M.; Urbakh, M.; Fineberg, J. Slip Sequences in Laboratory Experiments Resulting from Inhomogeneous Shear as Analogs of Earthquakes Associated with a Fault Edge. *Pure Appl. Geophys.* **2011**, *168*, 2151–2166.

6. Lhermerout, R.; Diederichs, C.; Perkin, S. Are Ionic Liquids Good Boundary Lubricants? A Molecular Perspective. *Lubricants* **2018**, *6*, 9.

7. Palacio, M.; Bhushan, B. A Review of Ionic Liquids for Green Molecular Lubrication in Nanotechnology. *Tribol. Lett.* **2010**, *40*, 247–268.

8. Glavatskih, S.; Höglund, E. Tribotronics–Towards Active Tribology. *Tribol. Int.* **2008**, *41*, 934–939.

9. Amiril, S.; Rahim, E.; Syahrullail, S. A Review on Ionic Liquids as Sustainable Lubricants in Manufacturing and Engineering: Recent Research, Performance, and Applications . *J. Clean. Prod.* **2017**, *168*, 1571–1589.

10. Minami, I. Ionic liquids in Tribology. *Molecules* **2009**, *14*, 2286–2305.

11. Smith, A. M.; Lovelock, K. R. J.; Gosvami, N. N.; Welton, T.; Perkin, S. Quantized Friction across Ionic Liquid Thin Films. *Phys. Chem. Chem. Phys.* **2013**, *15*, 15317–15320.

12. Fajardo, O. Y.; Bresme, F.; Kornyshev, A. A.; Urbakh, M. Electrotunable Lubricity with Ionic Liquid Nanoscale Films. *Sci. Rep.* **2015**, *5*, 7698.

13. Fajardo, O. Y.; Bresme, F.; Kornyshev, A. A.; Urbakh, M. Electrotunable Friction with Ionic Liquid Lubricants: How Important Is the Molecular Structure of the Ions? *J. Phys. Chem. Lett.* **2015**, *6*, 3998–4004.

14. Radiom, M. Ionic Liquid–Solid Interface and Applications in Lubrication and Energy Storage. *Curr. Opin. Colloid Interface Sci.* **2019**, *39*, 148–161.

15. Sweeney, J.; Hausen, F.; Hayes, R.; Webber, G. B.; Endres, F.; Rutland, M. W.; Bennewitz, R.; Atkin, R. Control of Nanoscale Friction on Gold in an Ionic Liquid by a Potential–Dependent Ionic Lubricant Layer. *Phys. Rev. Lett.* **2012**, *109*, 155502.

16. Li, H.; Wood, R. J.; Rutland, M. W.; Atkin, R. An Ionic Liquid Lubricant Enables Superlubricity to be "Switched on" in situ Using an Electrical Potential. *Chem. Comm.* **2014**, *50*, 4368–4370.

17. He, S.; Meng, Y.; Tian, Y. Correlation Between Adsorption/Desorption of Surfactant and Change in Friction of Stainless Steel in Aqueous Solutions Under Different Electrode Potentials. *Tribol. Lett.* **2011**, *41*, 485–494.

18. Smith, A. M.; Parkes, M. A.; Perkin, S. Molecular Friction Mechanisms Across Nanofilms of a Bilayer-Forming Ionic Liquid. *J. Phys. Chem. Lett.* **2014**, *5*, 4032–4037.

19. Capozza, R.; Benassi, A.; Vanossi, A.; Tosatti, E. Electrical Charging Effects on the Sliding Friction of a Model Nano–Confined Ionic Liquid. *J. Chem. Phys.* **2015**, *143*, 144703.

20. Fedorov, M. V.; Kornyshev, A. A. Ionic Liquids at Electrified Interfaces. *Chem. Rev.* **2014**, *114*, 2978–3036.

21. Monolayer to Bilayer Structural Transition in Confined Pyrrolidinium-Based Ionic Liquids.

22. Krämer, G.; Bennewitz, R. Molecular Rheology of a Nanometer-Confined Ionic Liquid. *J. Phys. Chem. C* **2019**, *123*, 28284–28290.

23. David, A.; Fajardo, O. Y.; Kornyshev, A. A.; Urbakh, M.; Bresme, F. Electrotunable Lubricity with Ionic Liquids: the Influence of Nanoscale Roughness. *Faraday Discuss.* **2017**, *199*, 279–297.

24. Fajardo, O.; Di Lecce, S.; Bresme, F. Molecular Dynamics Simulation of Imidazolium C_nMIM-BF4 Ionic Liquids using a Coarse Grained Force–Field. *Phys. Chem. Chem. Phys.* **2019**,

25. Gardas, R. L.; Freire, M. G.; Carvalho, P. J.; Marrucho, I. M.; Fonseca, I. M. A.; Ferreira, A. G. M.; Coutinho, J. A. P. PρT Measurements of Imidazolium-Based Ionic Liquids. *J. Chem. Eng. Data* **2007**, *52*, 1881–1888.

26. *Electrochemical Aspects of Ionic Liquids*; Wiley Interscience: Hoboken, N.J., 2005.

27. Bussi, G.; Donadio, D.; Parrinello, M. Canonical Sampling through Velocity Rescaling. *J. Chem. Phys.* **2007**, *126*, 014101.

28. Merlet, C.; Salanne, M.; Rotenberg, B. New Coarse-Grained Models of Imidazolium Ionic Liquids for Bulk and Interfacial Molecular Simulations. *J. Phys. Chem. C* **2012**, *116*, 7687–7693.

29. Zhou, H.; Rouha, M.; Feng, G.; Lee, S. S.; Docherty, H.; Fenter, P.; Cummings, P. T.; Fulvio, P. F.; Dai, S.; McDonough, J.; Presser, V.; Gogotsi, Y. Nanoscale Perturbations

of Room Temperature Ionic Liquid Structure at Charged and Uncharged Interfaces. *ACS Nano* **2012**, *6*, 9818–9827.

30. Schlegel, M. L.; Nagy, K. L.; Fenter, P.; Cheng, L.; Sturchio, N. C.; Jacobsen, S. D. Cation Sorption on the Muscovite (0 0 1) Surface in Chloride Solutions using High-Resolution X-Ray Reflectivity. *Geochim. Cosmochim. Acta* **2006**, *70*, 3549–3565.

31. Essmann, U.; Perera, L.; Berkowitz, M. L.; Darden, T.; Lee, H.; Pedersen, L. G. A Smooth Particle Mesh Ewald Method. *J. Chem. Phys.* **1995**, *103*, 8577–8593.

32. Berendsen, H.; van der Spoel, D.; van Drunen, R. GROMACS: A Message–Passing Parallel Molecular Dynamics Implementation. *Comput. Phys. Commun.* **1995**, *91*, 43–56.

33. Lindahl, E.; Hess, B.; van der Spoel, D. GROMACS 3.0: A Package for Molecular Simulation and Trajectory Analysis. *Mol. Modeling Annual* **2001**, *7*, 306–317.

34. Canongia Lopes, J. N.; Pádua, A. A. Nanostructural Organization in Ionic Liquids. *J. Phys. Chem. B* **2006**, *110*, 3330–3335.

35. Vanossi, A.; Manini, N.; Urbakh, M.; Zapperi, S.; Tosatti, E. Colloquium: Modeling Friction: from Nanoscale to Mesoscale. *Rev. Mod. Phys.* **2013**, *85*, 529–552.

Graphical TOC Entry